Effect of Zinc Oxide Modification by Indium Oxide on Microstructure, Adsorbed Surface Species, and Sensitivity to CO

Artem Marikutsa[1]*, Marina Rumyantseva[1], Alexander Gaskov[1], Maria Batuk[2], Joke Hadermann[2], Nasrin Sarmadian[3], Rolando Saniz[3], Bart Partoens[3] and Dirk Lamoen[3]

[1] Department of Chemistry, Moscow State University, Moscow, Russia, [2] EMAT, Departement of Physics, University of Antwerp, Antwerp, Belgium, [3] CMT, Departement of Physics, University of Antwerp, Antwerp, Belgium

Additives in semiconductor metal oxides are commonly used to improve sensing behavior of gas sensors. Due to complicated effects of additives on the materials microstructure, adsorption sites and reactivity to target gases the sensing mechanism with modified metal oxides is a matter of thorough research. Herein, we establish the promoting effect of nanocrystalline zinc oxide modification by 1–7 at.% of indium on the sensitivity to CO gas due to improved nanostructure dispersion and concentration of active sites. The sensing materials were synthesized via an aqueous coprecipitation route. Materials composition, particle size and BET area were evaluated using X-ray diffraction, nitrogen adsorption isotherms, high-resolution electron microscopy techniques and EDX-mapping. Surface species of chemisorbed oxygen, OH-groups, and acid sites were characterized by probe molecule techniques and infrared spectroscopy. It was found that particle size of zinc oxide decreased and the BET area increased with the amount of indium oxide. The additive was observed as amorphous indium oxide segregated on agglomerated ZnO nanocrystals. The measured concentration of surface species was higher on In_2O_3-modified zinc oxide. With the increase of indium oxide content, the sensor response of ZnO/In_2O_3 to CO was improved. Using *in situ* infrared spectroscopy, it was shown that oxidation of CO molecules was enhanced on the modified zinc oxide surface. The effect of modifier was attributed to promotion of surface OH-groups and enhancement of CO oxidation on the segregated indium ions, as suggested by DFT in previous work.

Keywords: zinc oxide, indium oxide, semiconductor gas sensor, carbon monoxide, surface modification, active sites

INTRODUCTION

Zinc oxide is an *n*-type semiconductor with band gap 3.2 eV that is of interest for resistive gas sensors (Kołodziejczak-Radzimska and Jesionowski, 2014). Doping by M(III) cations (Al, Ga, In) soluble in bulk Zno is commonly used to improve electronic conduction in nanocrystalline zinc oxide (Pearton et al., 2005; Ellmer, 2010; Kołodziejczak-Radzimska and Jesionowski, 2014). It has also been observed that dopants influence the sensitivity of zinc oxide to various target gases

(Han et al., 2009; Kim et al., 2009; Phan and Chung, 2013; Hou and Jayatissa, 2014; Hjiri et al., 2015; Nulhakim et al., 2017; Vorobyeva et al., 2017). Understanding the effect of dopants on gas sensing requires a description of the chemical processes in gas-solid interactions, i.e., target molecule adsorption and redox reaction of the adsorbate with the surface. Such descriptions are usually lacking in literature, since most studies are focused on the electronic properties of doped zinc oxide (Han et al., 2009; Hou and Jayatissa, 2014; Vorobyeva et al., 2017). Among the chemical aspects to be taken into account, there is information on active sites on the surface of the sensing material, adsorption sites for particular gas molecules and reactivity of the surface in redox interaction with the target gas. For example, the sensitivity of Ga-doped ZnO to acceptor NO$_2$ molecules was correlated to the concentration of paramagnetic donor sites in the materials, while a detrimental effect on the response to H$_2$S was established because of increased surface acidity (Vorobyeva et al., 2013).

Besides bulk doped materials, heterostructures of ZnO with M(III) oxides are often obtained. The nanocomposites ZnO/In$_2$O$_3$ have been synthesized with different morphologies and in a wide composition range for the use as gas sensors (Rambu et al., 2011; Singh et al., 2011; Lee et al., 2013, 2017; Trakhtenberga et al., 2013; Ma et al., 2016; Espid and Taghipour, 2017; Ilin et al., 2017; Wang et al., 2017; Wei et al., 2017; Zou et al., 2017; Choo et al., 2018; Guo et al., 2018; Liu et al., 2018), humidity sensors (Liang et al., 2012), photocatalysts (Wei et al., 2017; Markova et al., 2018), UV-light detectors (Wang et al., 2009). The studies of gas sensor behavior suggested the increased gas sensitivity of composites, in comparison to pure oxides. The increased sensitivity was revealed either to reducing analyte gases like hydrogen (Trakhtenberga et al., 2013; Ilin et al., 2017; Choo et al., 2018), ammonia (Rambu et al., 2011) and (CH$_3$)$_3$N (Lee et al., 2013), volatile organic compounds (Singh et al., 2011; Ma et al., 2016; Lee et al., 2017; Wang et al., 2017; Wei et al., 2017; Guo et al., 2018; Liu et al., 2018), or when the oxidizing gases were detected (Espid and Taghipour, 2017; Zou et al., 2017). The data on optimal Zn:In ratios in the gas sensors are contradictory and likely dependent on the synthesis procedure, materials morphology and microstructure and the properties of gas molecules to be detected. For example, improved sensitivity to butanol and chlorine was found for nanorods and nanoparticles of ZnO modified by In$_2$O$_3$ (3–4 at % indium) (Zou et al., 2017; Liu et al., 2018), while ZnO/In$_2$O$_3$ heterostructures with comparable molar fractions were established for sensing H$_2$ (Trakhtenberga et al., 2013; Ilin et al., 2017), trimethylamine (Lee et al., 2013) and NO$_2$ (Espid and Taghipour, 2017). The mechanism of sensitization due to the ZnO/In$_2$O$_3$ heterojunctions is most often speculated based on the electron band energy model at the interface between two oxides proposed in Markova et al. (2018). The increase of surface sensitivity to gases is rationalized in terms of potential barrier modification and charged double layer formation within the contact of ZnO/In$_2$O$_3$ phases (Singh et al., 2011; Ma et al., 2016; Wei et al., 2017; Guo et al., 2018). Nonetheless important is the influence of oxides adsorption, catalytic and acid-base properties (Lee et al., 2013, 2017; Trakhtenberga et al., 2013). Increment of active sites number at the composites surface due to oxygen

adsorption promoted by electronic effects in the ZnO/In$_2$O$_3$ junctions is often speculated as the reason for high sensitivity (Wang et al., 2017; Zou et al., 2017; Liu et al., 2018). However, no experimental evidences for the effect of materials composition on the surface active sites have yet been reported.

Carbon monoxide is a toxic gas to be obligatorily monitored in indoors and outdoors. Since the CO molecule has neither pronounced donor-acceptor nor acid-base properties, establishing the factors controlling sensitivity to carbon oxide is a challenge. Computational DFT-based methods are useful for estimating the possible surface sites, geometry and energetics of gas molecules adsorption, as demonstrated for pristine and Ga-doped ZnO models (Derakhshandeh and Anaraki-Ardakani, 2016). The task for the experimental investigation is to establish the relations between CO sensitivity and the effect of ZnO doping on the microstructure, active surface sites and the reactivity to the target gas.

This work is focused on the effect of zinc oxide modification by indium oxide on sensitivity and surface reactivity to CO. Saniz et al. (2018) reported on the DFT-modeling of impurity atoms formation in 4 wt.% In-doped Zno slabs, showing that the localization of In at the surface of zinc oxide is energetically favorable. It was found that the adsorption of CO and OH-species would be enhanced in the presence of In atoms on the surface. Moreover, interatomic bond elongation and charge transfer from the adsorbed CO molecule to the In-doped surface was predicted, suggesting that the electronic state of Zno would have improved sensitivity to CO (Saniz et al., 2018). Here we report on the experimental investigation of nanocrystalline In$_2$O$_3$-modified zinc oxide: materials microstructure, distribution of the additive, concentration of surface OH-species and chemisorbed oxygen, sensor response to CO and reactivity to the target gas in relation to the indium oxide amount in ZnO/In$_2$O$_3$. The sensitivity to CO correlated to the concentration of surface oxidizing species, OH-groups and to the reactivity of the surface to CO in presence of segregated In$_2$O$_3$ species, in agreement with the theoretical results in Saniz et al. (2018).

MATERIALS AND METHODS

Nanocrystalline zinc oxide modified by different amounts of In$_2$O$_3$ was synthesized via an aqueous coprecipitation route (Vorobyeva et al., 2013, 2017). The concentrations of In were 1, 3, 5, and 7 at %. Pristine ZnO was obtained as a reference sample. Solution of 1.23 M Zn(NO$_3$)$_2$ mixed with a calculated volume of 0.25 M In(NO$_3$)$_3$ solution was added to a 2-fold excess of 1.9 M NH$_4$HCO$_3$ solution and stirred at 50°C for 30 min, then left for 1 h at room temperature. The white precipitates of mixed zinc-indium basic carbonates were washed by deionized water and centrifuged, dried at 50°C overnight and annealed at 450°C in air for 24 h to obtain ZnO/In$_2$O$_3$ samples.

Phase composition and crystal structure were studied by X-ray diffraction using a DRON-4 instrument. The crystallite size (d_{XRD}) of ZnO was calculated from the broadening of the (100) peak using the Scherrer equation, wave length λ = 1.5406 Å (Cu K$_{\alpha1}$ radiation). Microstructure and indium oxide distribution

were studied by transmission electron microscopy (TEM). The materials were ultrasonically dispersed in ethanol and drop-deposited onto a Cu-grid covered with carbon. The TEM images and electron diffraction (ED) patterns were acquired on a FEI Osiris microscope operated at 200 kV. High angle annular dark field scanning transmission electron microscopy (HAADF-STEM) images and energy dispersive X-ray (EDX) maps were acquired using a FEI Titan 80–300 "cubed" microscope equipped with a Super-X detector and operated at 300 kV. The probe current was 200 pA. Zn-K, In-L, and O-K lines were used for the chemical maps.

The specific surface area was measured by low-temperature nitrogen adsorption (Brunauer-Emmett-Teller, BET method) on a Chemisorb 2,750 (Micromeritics) instrument. Cationic composition was determined with micro X-ray fluorescent (XRF) analysis on a Mistral M1 (Bruker) device, acceleration voltage 50 kV, scanning area 1.5 × 1.5 mm and accumulation 30 s. Surface hydroxyl species were analyzed using FTIR transmission spectra of samples pressed in KBr pellets. Spectra were registered in the 4,000–400 cm^{-1} range with a Frontier (Perkin Elmer) spectrometer. Temperature-programmed reduction by hydrogen was performed without pretreatment of the samples. The powders (~30 mg) were placed in a flow reactor through which H$_2$(10%):Ar was purged. Hydrogen consumption from gas flow was measured with a thermo-conductivity detector under heating to 900°C with a rate of 5°C/min.

Sensor measurements were performed using a laboratory setup consisting of an automatized electrometer with a flow chamber and gas-regulation system. The source of carrier gas was a generator of purified air, model "1,2–3,5" (Himelectronica, Russia), contamination levels within the limits of 10 ppm H$_2$O, 2 ppm CO$_2$, 0.1 ppm hydrocarbons. Certified gas mixtures of CO (1,050 ± 50 ppm):N$_2$, H$_2$ (1 ± 0.05%):N$_2$, CO$_2$ (10 ± 0.4%):air, NH$_3$ (1,600 ± 50 ppm):N$_2$, NO (100 ± 5 ppm):N$_2$, C$_6$H$_6$ (44 ± 4 ppm):N$_2$, SO$_2$ (98 ± 5 ppm):N$_2$, NO$_2$ (100 ± 7 ppm):N$_2$ (MGPZ, Russia) were used as the sources of test gases. Relative humidity of carrier gas was varied by mixing dry air and 100% RH humid air flows at room temperature and measured by humidity meter IVTM-7 (NTC-IGD, Russia). Gas concentrations and flows were controlled by EL-FLOW mass-flow controllers (Bronkhorst). Powders were ground with terpineol into a paste which was drop-deposited onto alumina microhotplates provided with vapor-deposited Pt-contacts and heater, forming a sensing layer sized 1 × 0.5 mm and 5–7 μm thick (**Supplementary Data**). Prior to measurements, the sensors were annealed at 350°C in air for 20 h to remove the binder. The sensor resistance was measured at DC-voltage 1.3 V under *in situ* controlled composition of gas flow (100 ml/min) at temperatures fixed in the range 25–450°C. The sensor signal was defined as the ratio of resistance in air (R_a) relative to that in test gas (R_g):

$$S = (R_a - R_g)/R_g. \tag{1}$$

Diffuse-reflectance infrared Fourier-transformed (DRIFT) spectra were collected using a Frontier (Perkin Elmer) spectrometer equipped with DiffusIR annex and a flow test chamber HC900 (Pik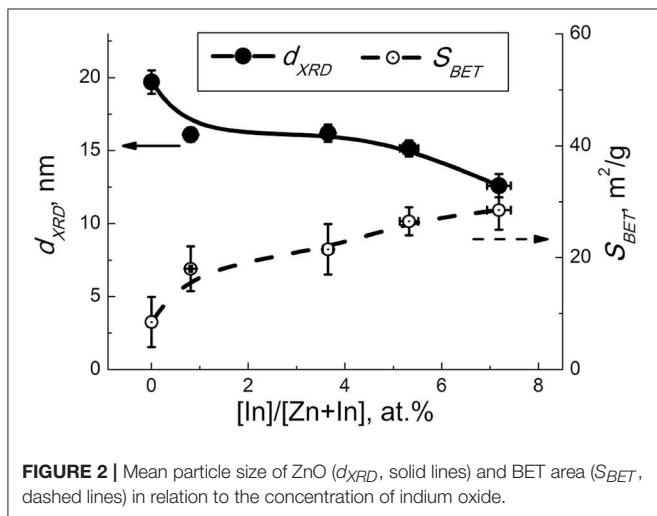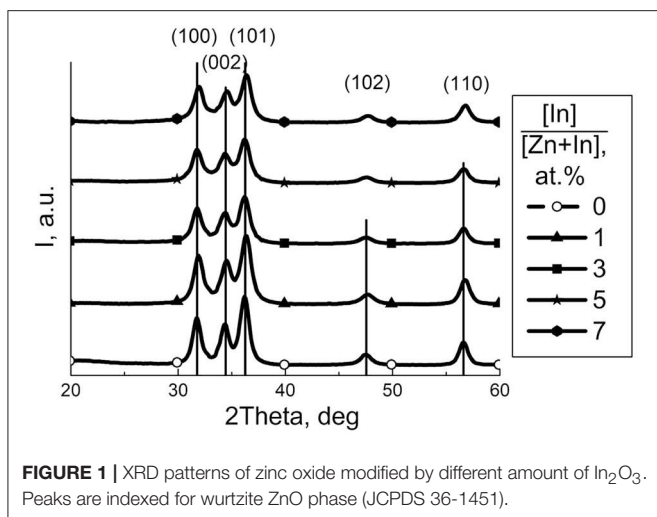e Technologies) with a heater and ZnSe window. Spectra were registered in the 4,000–1,000 cm^{-1} region, accumulating 30 scans at ambient conditions with automatic H$_2$O/CO$_2$ compensation. Powders (30 mg) were compressed in an alumina crucible (5 mm diameter). The surface acidity of the samples was compared under adsorption of NH$_3$ probe molecules (200 ppm in air, flow 100 ml/min) at room temperature. Before exposure to ammonia, the samples were heated in air at 150°C for 1 h to remove adsorbed water and then held at room temperature for 1 h. Interaction with test gases was studied under *in situ* exposure to CO (200 ppm), H$_2$ (200 ppm), and CO$_2$ (0.1 %) at 150° and 450°C after heating in air for 3 h at the same temperatures. DRIFT spectra in test gases were collected each 15 min for 1.5 h, relative to the background spectrum which was registered after the pretreatment.

RESULTS AND DISCUSSION

Materials Composition, Microstructure and Indium Oxide Distribution

The element composition of ZnO/In$_2$O$_3$ estimated by XRF agreed with the loaded indium amounts (1–7 at.%) within the measurement errors. According to X-ray diffraction, the samples of pure ZnO and modified ZnO/In$_2$O$_3$ contain a single crystalline phase, i.e., wurtzite-like zinc oxide (**Figure 1**). Because of peak broadening, any changes in unit cell parameters were within the refinement error interval. With the increase of indium oxide content, the mean crystallite size (d_{XRD}) of ZnO decreased and the BET surface area increased (**Figure 2**). This is due to inhibited crystallite growth during the thermal treatment of the co-precipitated metal hydroxocarbonates. Previously it was attributed to the formation of defects (interstitial cations $M_{Zn}^{\cdot\cdot}$, oxygen vacancies $V_O^{\cdot\cdot}$) and/or lattice distortions upon incorporation of In(III) into ZnO, because of the difference of ionic radii of Zn(II) (0.60 Å) and In(III) (0.62 Å) in tetrahedral coordination (Shannon, 1976). This assumption is in line with the change of Zn-O bond length following the introduction of In, as shown by DFT (Saniz et al., 2018). Previously, the solubility of In in similarly prepared nanocrystalline ZnO(In) was estimated to be 1 at.% In Vorobyeva et al. (2017). However, in the current study, TEM and EDX detected indium only in segregated form on the surface of ZnO. Hence, most likely the segregated additive blocked the diffusion of zinc and oxygen ions, hampering the crystallization of zinc oxide nanoparticles.

In HAADF-STEM images (**Figure 3a** and **Figure S2**) one can distinguish two types of material: agglomerated nanoparticles and porous spheres. The nanoparticles have a size of 8–30 nm and correspond to wurtzite-like ZnO phase, as confirmed by electron diffraction (inset in **Figure 3a**). The porous spheres range in size from 60 to 100 nm and correspond to In$_2$O$_3$. High resolution TEM images (**Figure 3b**) and EDX elemental mapping (**Figure 4**) allowed distinguishing the crystalline ZnO nanoparticles with ordered atomic planes from amorphous In$_2$O$_3$. No indium signal was detected on the EDX spectra of the ZnO/In$_2$O$_3$ (1 at % In) sample taken from the individual ZnO nanoparticles (areas 1, 2 in **Figure 4b**, spectra are in **Figure S3**). Yet, 1 at.% is below the detection limit of the
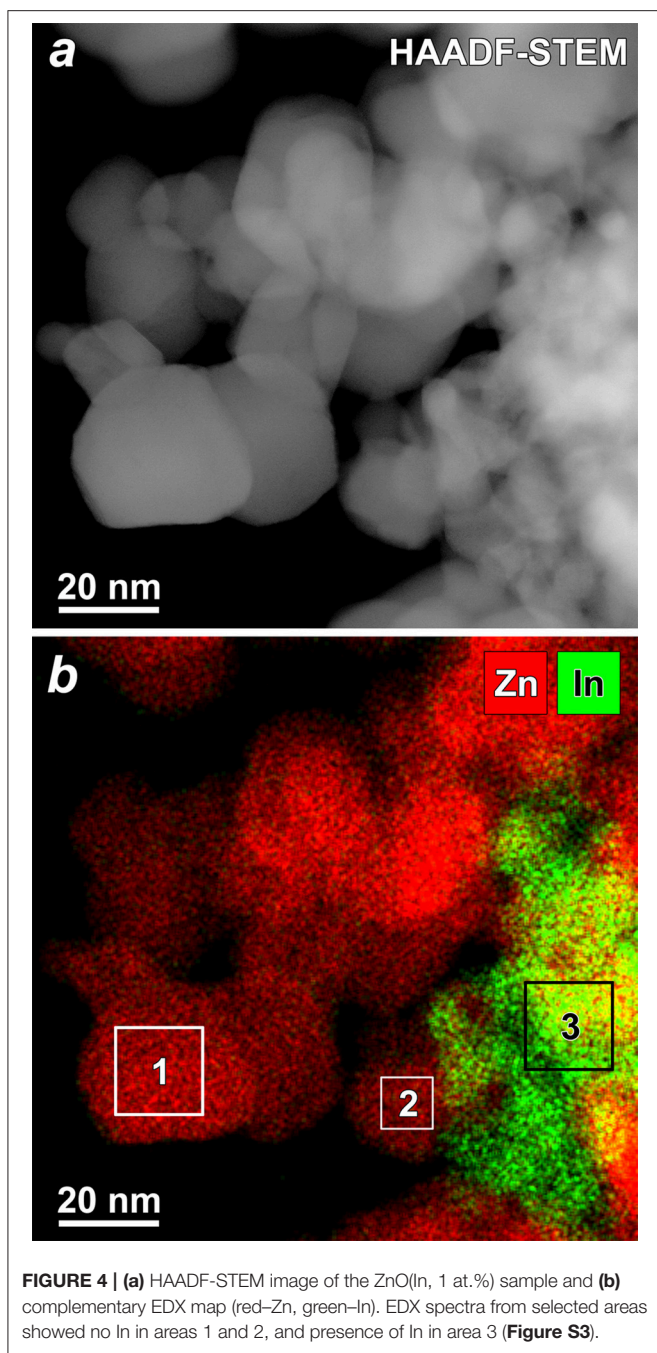
FIGURE 1 | XRD patterns of zinc oxide modified by different amount of In$_2$O$_3$. Peaks are indexed for wurtzite ZnO phase (JCPDS 36-1451).

FIGURE 2 | Mean particle size of ZnO (d_{XRD}, solid lines) and BET area (S_{BET}, dashed lines) in relation to the concentration of indium oxide.

FIGURE 3 | **(a)** HAADF-STEM image of the ZnO(In, 5 at.%) sample; inset–ring electron diffraction pattern acquired from the large area. The rings are completely indexed using wurtzite structure, (i.e., from center to periphery) 010; 002; 011; 012; −120; 013; −122. **(b)** HRTEM image of the ZnO(In, 5 at.%) sample showing individual crystalline ZnO particle and amorphous In$_2$O$_3$ (corresponding FFT's are inserted).

technique and cannot be seen on the spectra. Since indium oxide is abundantly present as an amorphous segregation in all the studied ZnO/In$_2$O$_3$ materials, it is possible that there is effectively no indium in the ZnO nanoparticles. A failure to incorporate In(III) in the ZnO lattice could be explained by the preference of In(III) for an octahedral oxygen coordination (Shannon, 1976). Furthermore, the annealing temperature of 450°C might be not enough for the elimination of amorphous phase and crystallization of ZnO(In) as a solid solution. Noteworthy, the preferred segregation of In atoms on a model ZnO surface, rather than incorporation into the bulk, was suggested by first-principles calculations (Saniz et al., 2018).

## Effect of Additive on Surface Species of ZnO/In$_2$O$_3$

Hydroxyl species on the surface of materials were examined by FTIR spectroscopy. The spectra (**Figure 5A**) consist of peaks relevant to lattice ZnO (420–460 cm^{-1}) and surface Zn-O (800–1,200 cm^{-1}) vibrations (Davydov, 2003) and/or phonon
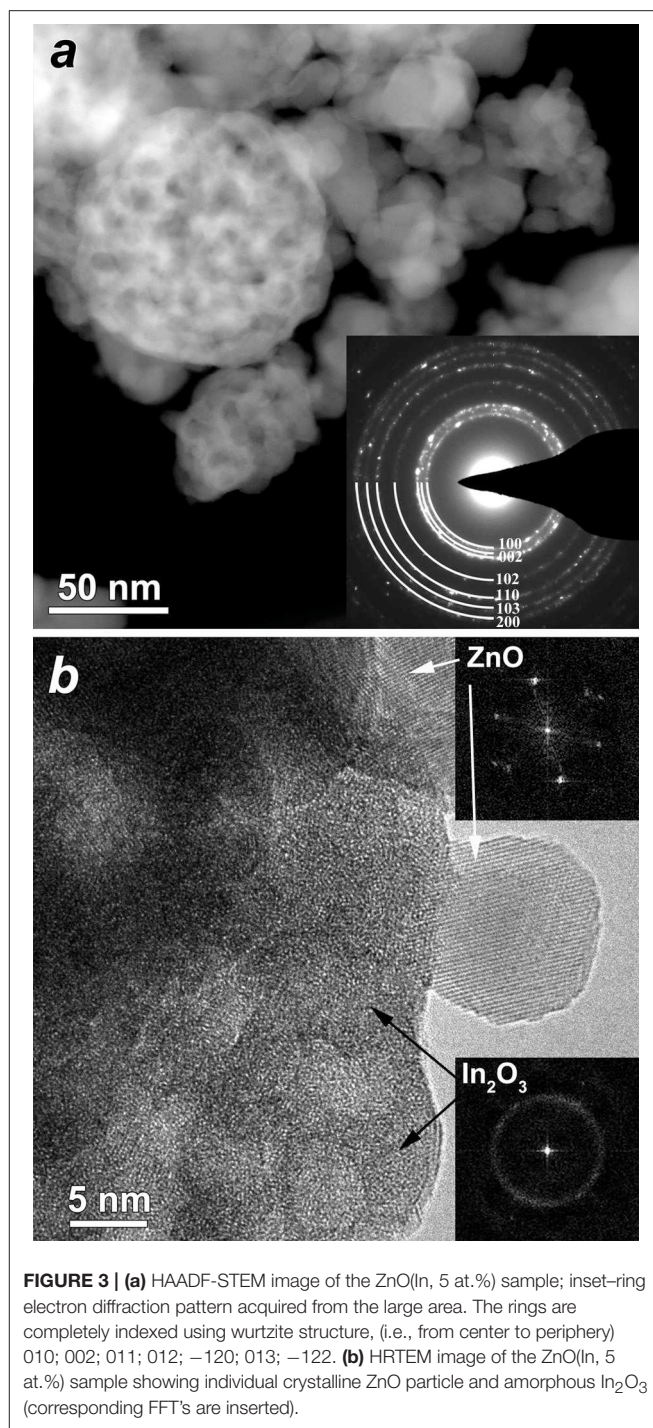
mode vibrations of ZnO (700–1,100 cm^{-1}) (Boccuzzi et al., 1981). The multicomponent bands at 1,300–1,700 cm^{-1} can be contributed by bending vibrations of adsorbed H$_2$O (1650 cm^{-1}) and surface Zn-O-H groups (1,320, 1,395, 1,410, 1,560, 1,605, and 1,640 cm^{-1}; Keyes et al., 2005) as well as carbonate (1,350 and 1,530 cm^{-1}; Boccuzzi et al., 1979), hydrocarbonate (1,635 cm^{-1}; Saussey et al., 1982) or adsorbed CO$_2$ (1,370 cm^{-1}; Saussey et al., 1982; 1,360–1,450 cm^{-1}, 1,540–1,650

FIGURE 4 | (a) HAADF-STEM image of the ZnO(In, 1 at.%) sample and (b) complementary EDX map (red–Zn, green–In). EDX spectra from selected areas showed no In in areas 1 and 2, and presence of In in area 3 (Figure S3).

FIGURE 5 | (A) FTIR transmission spectra of zinc oxide modified by different amount of In$_2$O$_3$. (B) IR absorbance at OH-stretching vibrational peak (3,400 cm^{-1}) normalized to that at lattice Zn-O peak (460 cm^{-1}) in relation to the content of indium oxide in ZnO/In$_2$O$_3$.
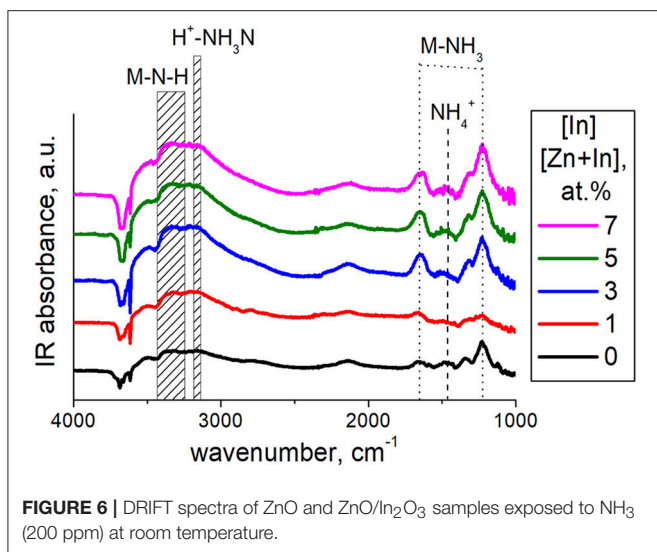
cm^{-1}; Keyes et al., 2005). The wide band of stretching O–H vibrations at 2,400–3,700 cm^{-1} is indicative of a wide range of hydrated surface species including separate OH-groups (3,500–3,700 cm^{-1}; Atherton et al., 1971; Keyes et al., 2005), hydrogen-bound groups OH…OH at 3,400 cm^{-1} (Atherton et al., 1971), and OH-groups associated with zinc vacancies (3,220–3,230 cm^{-1}; Keyes et al., 2005). The main difference in the spectra of the modified samples was in the relative intensities of hydroxyl-related bands at 3,700–2,400 cm^{-1} and 1,700–1,300 cm^{-1}. In Figure 5B the intensity of the most prominent O-H band (3,400 cm^{-1}) normalized by that of lattice ZnO vibrations (420–460
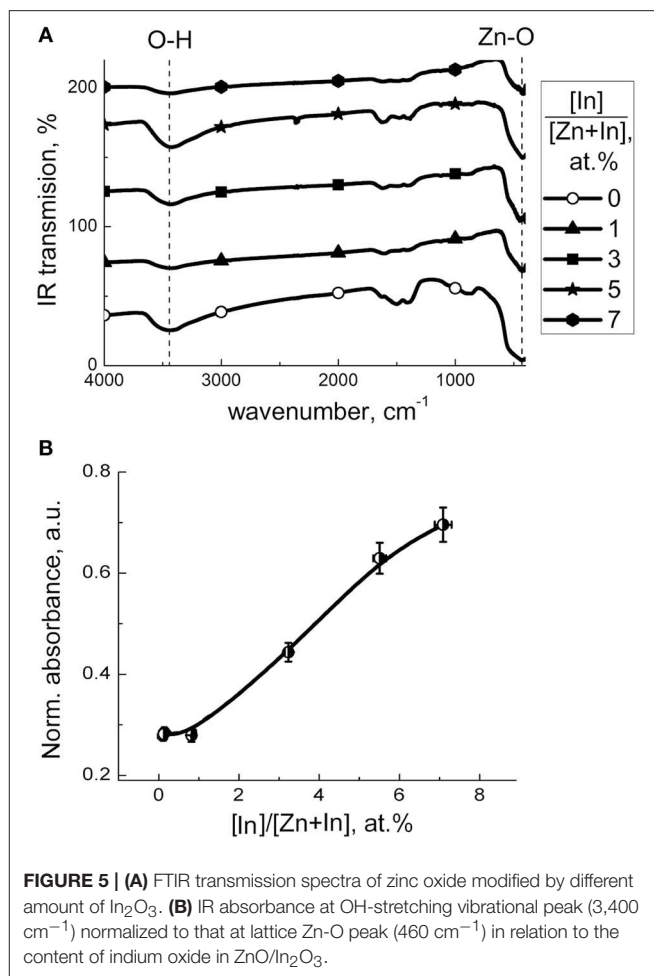
cm^{-1}) is plotted in relation to sample composition. It suggests that the concentration of surface OH-species increased with the content of indium oxide. The hydration could be due to an increasing number of In(III)-ions segregated on the surface, which is in agreement with the higher OH adsorption energy on doped ZnO(In) surface, as theoretically suggested (Saniz et al., 2018). From the chemical point of view, it originates from increased chemisorption of donor H$_2$O molecules on triple-charged positive In(III) cations at the surface of ZnO. By DRIFT spectroscopy of probe NH$_3$ molecules adsorption, it was shown that the acidity of modified zinc oxide increased with the content of indium oxide (Figure 6). The intensities of the bands corresponding to stretching N-H vibrations (3,260–3,380 cm^{-1}; Morimoto et al., 1976; Belokopytov et al., 1979) and bending NH$_3$ vibrations (symmetric 1,610 cm^{-1}, asymmetric 1,255 cm^{-1}; Belokopytov et al., 1979) of cation-bound NH$_3$ and those of OH-bound NH$_4^+$ species (stretching 3,200 cm^{-1}, symmetric bending 1,455 cm^{-1}; Morimoto et al., 1976) increased with the amount of indium oxide.
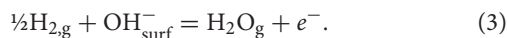
Temperature profiles of hydrogen consumption during temperature-programmed reduction (TPR) of the materials are shown in Figure 7A. Prominent hydrogen consumption was detected at temperature 150–600°C, but bulk reduction of ZnO

FIGURE 6 | DRIFT spectra of ZnO and ZnO/In$_2$O$_3$ samples exposed to NH$_3$ (200 ppm) at room temperature.

was not achieved on heating to 900°C. In the lower-temperature range 150–450°C the consumption of H$_2$ is attributable to the reduction of chemisorbed oxygen species (Marikutsa et al., 2013):
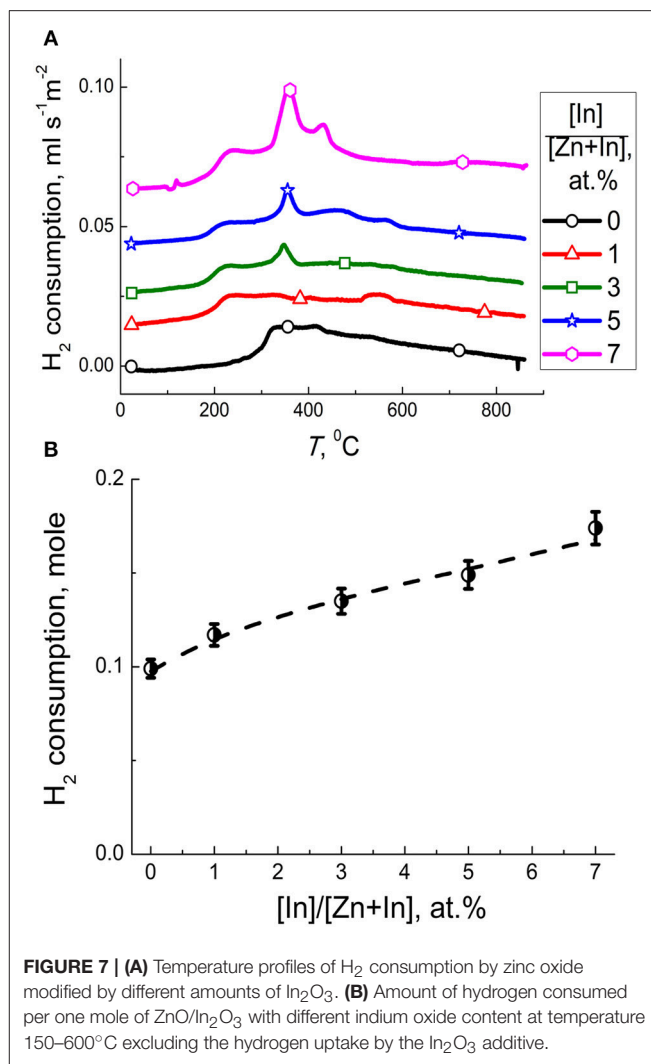
$$mH_{2,g} + O^{n-}_{m\ surf} = mH_2O_g + ne^-. \qquad (2)$$
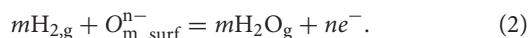
where m and n designates the kind of oxygen surface species, which depends on temperature: O_2^- at temperature below 200°C, O^- – at temperature 200–400°C and O^{2-} – at temperature higher than 400°C (Chon and Pajares, 1969). Reduction of hydroxyl surface species can also take place in the lower-temperature range:

$$\tfrac{1}{2}H_{2,g} + OH^-_{surf} = H_2O_g + e^-. \qquad (3)$$

The consumption of hydrogen at temperature higher than 450°C must be due to a partial reduction of ZnO and of segregated In$_2$O$_3$ phase on the surface of ZnO/In$_2$O$_3$:

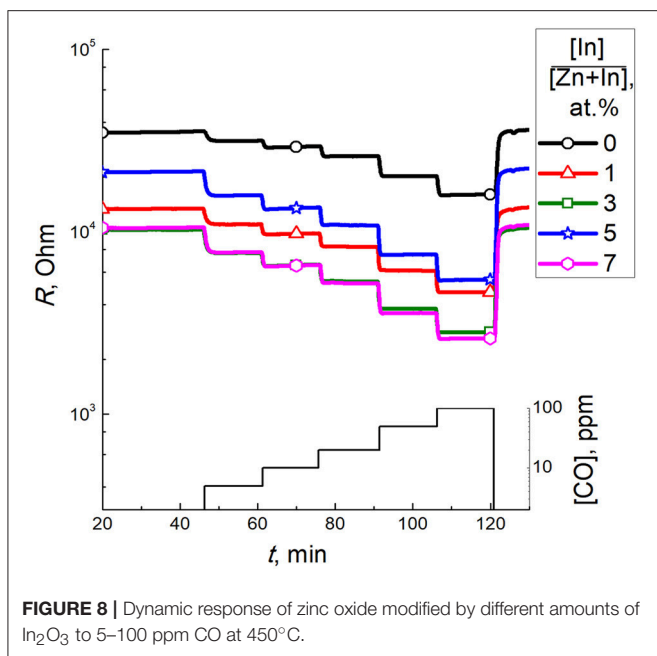$$3H_{2,g} + In_2O_{3,s} = 3H_2O_g + 2In_l. \qquad (4)$$
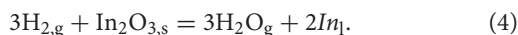
The profile of ZnO/In$_2$O$_3$ (1 at.% In) was similar to that of the pristine ZnO. With the increase of indium content to 3–7 at % In, the peaks of H$_2$ consumption at 150–600°C increased (**Figure 7A**). It can be due to the increase of indium oxide content and the increase of surface coverage by chemisorbed oxygen species. To distinguish the effect of reducible surface species we subtracted the amount of H$_2$ needed for reduction of present amounts of In$_2$O$_3$ in the samples from the total hydrogen consumption in this temperature range. The results (**Figure 7B**) show that hydrogen consumption by the samples still increased with the In$_2$O$_3$ content in ZnO/In$_2$O$_3$, although the uptake by the In$_2$O$_3$ was excluded. Thus, the concentration of reducible chemisorbed species on the surface of zinc oxide was likely increased due to the modification by indium oxide. The promotion of oxygen chemisorption should be due to the influence of segregated In$_2$O$_3$. Indium oxide is an n-type semiconductor with the intrinsic defects being oxygen

FIGURE 7 | (A) Temperature profiles of H$_2$ consumption by zinc oxide modified by different amounts of In$_2$O$_3$. **(B)** Amount of hydrogen consumed per one mole of ZnO/In$_2$O$_3$ with different indium oxide content at temperature 150–600°C excluding the hydrogen uptake by the In$_2$O$_3$ additive.

vacancies (Korotcenkov et al., 2016). The junction model between crystalline ZnO and In$_2$O$_3$ oxides predicts that electron-enriched layer is formed in ZnO that favors chemisorption of acceptor O$_2$ molecules, as had been expected in other works (Wang et al., 2017; Zou et al., 2017; Liu et al., 2018). An alternative reason for higher oxygen coverage can be the larger surface area of the modified samples (**Figure 2**).

Sensing Behavior to CO

Figure 8 shows dynamic response of the sensors to different concentrations of CO. At all temperatures tested, the baseline resistance in air was highest for pristine ZnO and decreased non-monotonously with increasing In$_2$O$_3$ content. Sensors responses were stable and reproducible, as shown by continuous tests at fixed temperature and CO concentration (dynamic response plot is shown in **Supplementary data**) and repeated tests with the same sensors after several weeks of delay. For the modified sensors, the temperature dependence of the sensor signal to a fixed CO concentration (5 ppm) increased with temperature to 450°C (**Figure 9A**), showing a local maximum at ∼150°C.

FIGURE 8 | Dynamic response of zinc oxide modified by different amounts of In$_2$O$_3$ to 5–100 ppm CO at 450°C.

FIGURE 9 | (A) Sensor signal of zinc oxide modified by different amounts of In$_2$O$_3$ to 5 ppm CO as a function of temperature. **(B)** Sensor signal of modified zinc oxide to 5 ppm CO at 150°C (solid lines) and 450°C (dashed lines) as a function of In content.

Similar to previous research, the increase of CO sensitivity upon heating to high temperature could be assigned to thermal activation of the reaction of CO with chemisorbed oxygen (Kim et al., 2009; Hjiri et al., 2015; Lim et al., 2015). However, heating to 150°C would be insufficient for thermal activation. In this case the redox reaction at the surface of modified zinc oxide could be facilitated via CO adsorption. As theoretically shown, the In atoms localized at the surface of ZnO should favor CO adsorption and loosen the interatomic C-O bond in the adsorbate (Saniz et al., 2018). This should lower the activation energy for oxidation of adsorbed CO:

$$2CO + O_{2\ surf}^- = 2CO_{2,g} + e^-. \qquad (5)$$
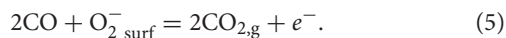
Taking into account the entropy factor, inhibition of CO adsorption at raised temperature may account for the decline of the sensor signal on heating to ∼200°C (**Figure 9A**). Further increase of sensor response at 200–450°C can be either due to thermal activation of the redox reaction, or due to transformation of predominant surface oxygen species into more reactive atomic forms (Chon and Pajares, 1969).
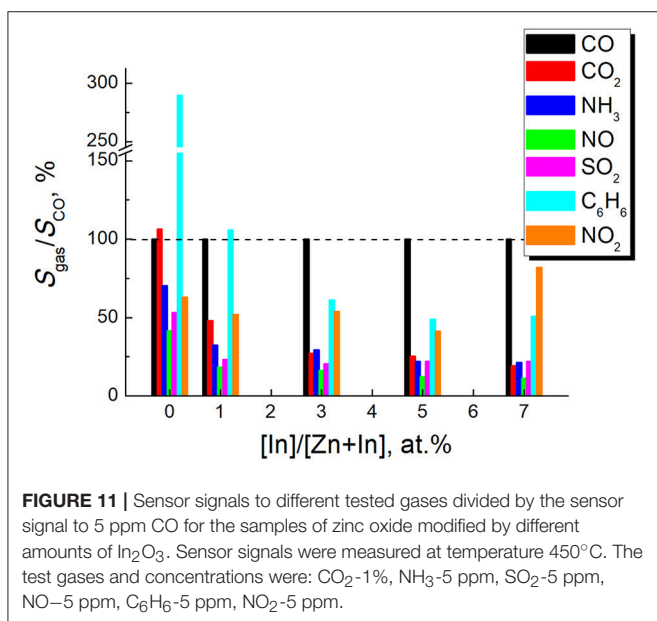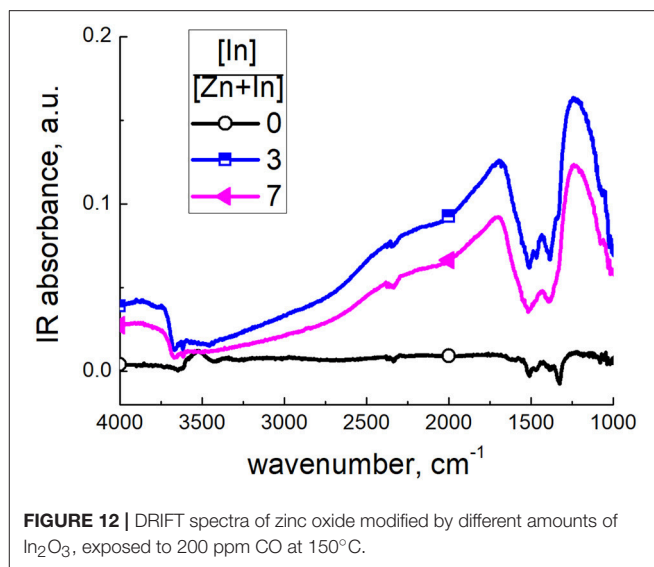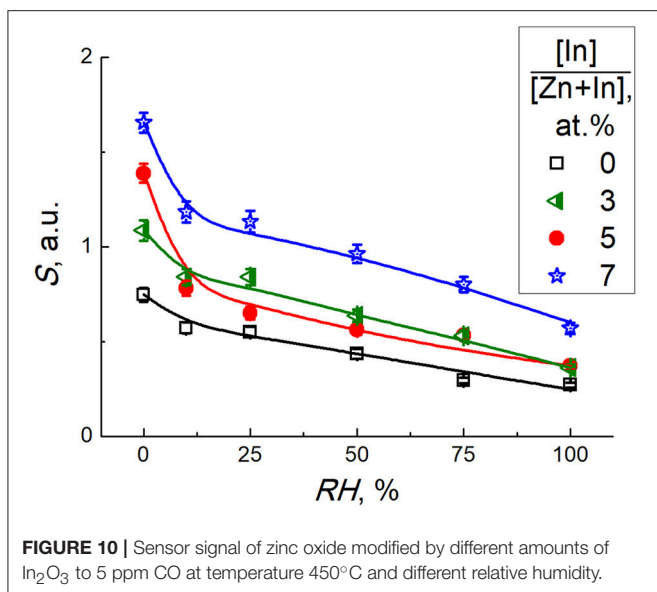
As follows from the plot of sensor signal vs. indium oxide content in zinc oxide, the sensitivity to CO increased with the concentration of additive (**Figure 9B**). The factor of microstructure (lower particle size, larger BET area) could not be excluded from the effect of the additive on the sensitivity of nanocomposites. Considering the role of surface chemistry in the reception of target molecules, the promotion of sensitivity to CO on increasing In$_2$O$_3$ content in ZnO/In$_2$O$_3$ agrees both with the increased concentration of chemisorbed oxygen, and with the In-cations being favorable adsorption sites for CO molecules as inferred from DFT (Saniz et al., 2018). The role of surface acidity of ZnO/In$_2$O$_3$ inferred from DRIFT
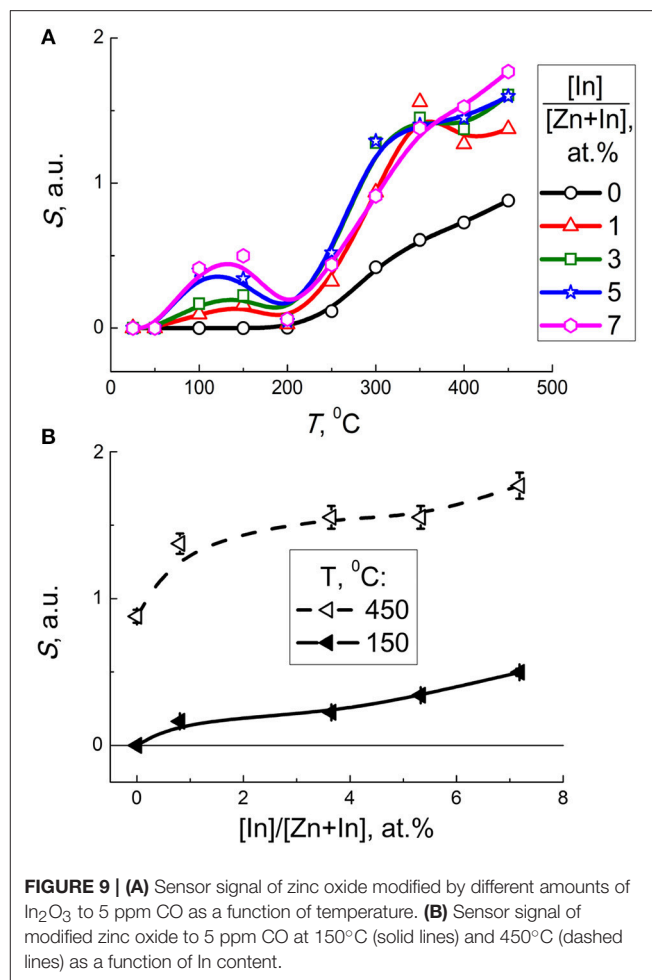
and FTIR data discussed above might also contribute to CO sensitivity, e.g., via the interaction of target gas with active surface OH-groups.

Sensor response to CO decreased with the increase of relative humidity (**Figure 10**). Dynamic response to 5 ppm CO at different humidity is provided in **Supplementary Data**. It can be explained by competing water molecules adsorption and blocking the active sites of CO adsorption and oxidation. The drop of sensitivity was larger for the sensors with higher In$_2$O$_3$ content (5–7 at.% In), in accordance with the higher surface acidity and water adsorption capacity of these ZnO/In$_2$O$_3$ samples inferred from FTIR data.

Selectivity of the sensor response to CO was compared to different interfering gases. For this purpose, the sensor signals to 5 ppm or a higher concentration of a test gas were divided by the signal to 5 ppm CO measured at 450°C for each sensor (**Figure 11**). The dynamic sensor responses are in **Supplementary Data**. As follows from the data in **Figure 11**, the least selectivity was demonstrated by pure ZnO: the cross-sensitivity to benzene was 3 times higher than to CO and the signals to other gases tested were not < 50% of the signal to CO. However, for the samples ZnO/In$_2$O$_3$ with 3–7 at % indium content the sensor signals to most of tested

FIGURE 10 | Sensor signal of zinc oxide modified by different amounts of In$_2$O$_3$ to 5 ppm CO at temperature 450°C and different relative humidity.

FIGURE 12 | DRIFT spectra of zinc oxide modified by different amounts of In$_2$O$_3$, exposed to 200 ppm CO at 150°C.

FIGURE 11 | Sensor signals to different tested gases divided by the sensor signal to 5 ppm CO for the samples of zinc oxide modified by different amounts of In$_2$O$_3$. Sensor signals were measured at temperature 450°C. The test gases and concentrations were: CO$_2$-1%, NH$_3$-5 ppm, SO$_2$-5 ppm, NO−5 ppm, C$_6$H$_6$-5 ppm, NO$_2$-5 ppm.

interfering gases were below 25% of the sensor signals to CO, except the interference from benzene and nitrogen dioxide. The persistent cross-sensitivity to NO$_2$ is unproblematic, since it is an oxidizing gas in contrast to the other reducing gases tested. These types of analytes can be discriminated by the direction of resistance response (increase or decrease) of the n-type ZnO/In$_2$O$_3$ samples.

DRIFT Study of Interaction With CO

The interaction with CO was probed by DRIFT spectroscopy at a temperature corresponding to higher sensitivity. The spectra of zinc oxide exposed to CO at 150°C displayed negative IR absorption peaks at 1,510 and 1,330 cm^{-1} and increased baseline absorption in case of modified samples (**Figure 12**). The intensity

of spectral changes corresponded to the CO concentration (100–200 ppm) and recovered the initial state in 1 h after the end of exposure to CO. Modulation of the baseline can be due to increasing charge density in the semiconductor oxide following the adsorption and redox interaction with CO (Equation 5), both resulting in charge transfer from adsorbate to the surface. Moreover, its variation is consistent with higher conductivity of modified zinc oxide (**Figure 8**). The origin of the negative band at 1,690–1,280 cm^{-1} is unclear. It matches the range of bending Zn-O-H vibrations, adsorbed carbonate, CO$_2$ and water molecules, as discussed above. However, were it due to carbonate, there should have been positive IR absorbance in the presence of CO. Furthermore, the dynamic behavior of this spectral feature was simultaneous with the baseline variation. Thus, this band could be related to the change of electronic state of the materials exposed to CO.

Interaction with CO at 450°C resulted in the same DRIFT spectral features, as at lower temperature, except for the appearance of sharp peaks at 1,510 and 1,320 cm^{-1} (**Figure 13A**). These positive peaks overlapped with the negative absorption band in the presence of CO, more for modified zinc oxide. However, these bands had different dynamic behavior. As demonstrated in **Figure 13B**, the baseline shift and negative band almost disappeared within 15 min after the end of the exposure to CO. However, the pair of sharp peaks at 1,510 and 1,320 cm^{-1} remained for this period, and disappeared only in 60–90 min after the end of CO exposure. These peaks are relevant to stretching vibrations of bidentate carbonate groups (Nakamoto, 1986). This attribution was confirmed by the comparison of DRIFT spectra of materials interacting with CO$_2$ gas (**Figure 13C**). The peak intensities were higher for modified ZnO/In$_2$O$_3$ in agreement with the higher CO sensitivity, as opposed to pristine ZnO. However, comparing the spectra of the sample with higher In$_2$O$_3$ content (7 at % In) it is seen that carbonate peaks formed in presence of CO (**Figure 13A**) disappeared within 15 min after CO flow was stopped (**Figure 13B**). That carbonate species
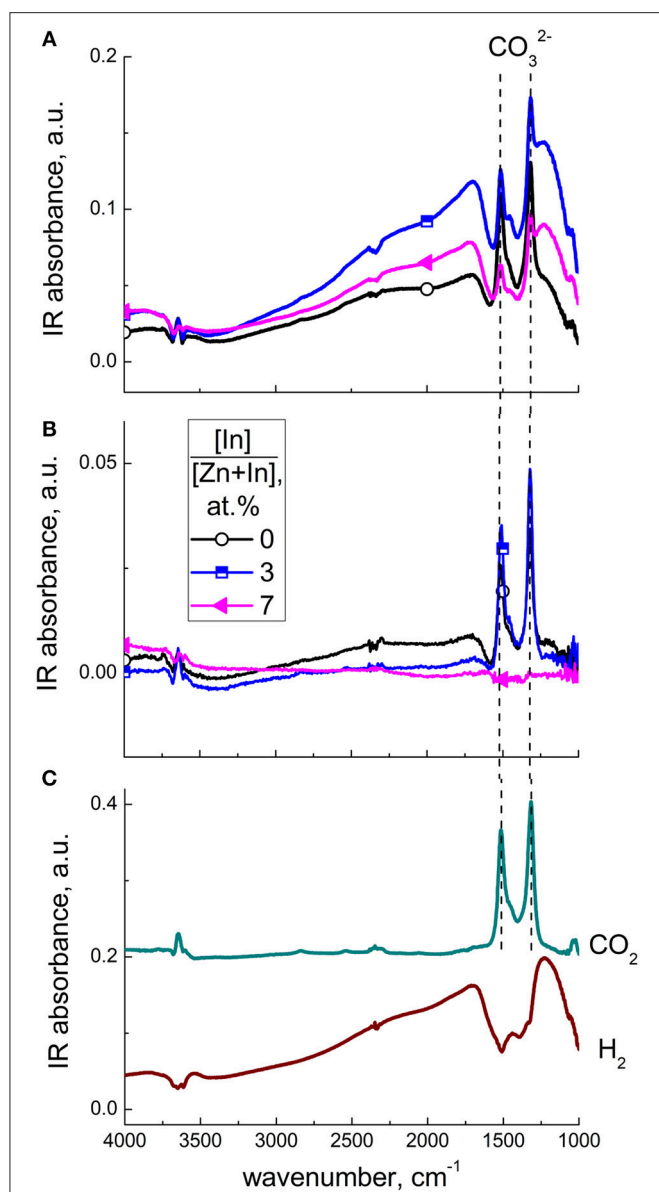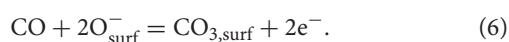
FIGURE 13 | DRIFT spectra of zinc oxide modified by different amounts of In$_2$O$_3$, exposed to 200 ppm CO at 450°C **(A)** and to air, 15 min after the end of CO exposure **(B)**. DRIFT spectra of ZnO(In, 3 at.%) exposed to 200 ppm H$_2$ and 0.1 % CO$_2$ at 450°C **(C)**.

disappeared from this sample readily while retained for this period on pure ZnO and ZnO/In$_2$O$_3$ with 3 at.% In content can be attributed to the increasing surface acidity of the samples with increasing indium oxide content, as discussed in section Effect of additive on surface species of ZnO/In2O3. The higher metal oxide acidity is favorable for carbonate decomposition and evolution of acidic CO$_2$. Thus, the interaction of pristine and In$_2$O$_3$-modified zinc oxide with CO at higher temperature could be formulated taking into account the predominant surface oxygen type as:

$$CO + 2O_{surf}^- = CO_{3,surf} + 2e^-. \qquad (6)$$

From the comparison of DRIFT spectra of modified zinc oxide exposed to CO (**Figure 13A**) and H$_2$ (**Figure 13C**) at 450°C the same observations were made, i.e., fast and reversible (within 15 min) increase of baseline IR absorption accompanied by a negative band at 1,690–1,280 cm^{-1}. Since the interaction with H$_2$ could not produce any carbonate species and the reversible behavior of Zn-OH groups at such high temperature is unlikely, these spectral features seem to be characteristic of solid-state behavior of modified zinc oxide in the presence of reducing gas molecules.

CONCLUSIONS

Nanocrystalline zinc oxide modified by In$_2$O$_3$ (0–7 at % In) was obtained via coprecipitation and annealing at 450°C. By XRD, BET, and TEM analyses it was shown that the modified samples had lower particle size of wurtzite-like ZnO and larger surface area. The additive was observed as amorphous In$_2$O$_3$ segregated on the agglomerations of ZnO nanoparticles. No solubility in bulk zinc oxide being detected. This coincides with the DFT-predicted preference of In adatoms to be located at the surface, rather than in the bulk of a model ZnO structure. It was demonstrated, that on raising the indium oxide content, the concentration of chemisorbed oxygen and surface OH-species increased on the surface of nanocrystalline ZnO/In$_2$O$_3$. The sensor response to 5–100 ppm CO in air improved due to ZnO modification by In$_2$O$_3$. Promotion of CO adsorption on segregated indium oxide species was assumed as the reason for the improved sensitivity at 150°C, in agreement with the effect inferred from DFT modeling of target molecules adsorption. Equally important, the improved sensitivity was in line with the influence of the additive on the materials microstructure and on the concentration of active oxygen and OH-species on the surface of ZnO/In$_2$O$_3$. The interaction with CO at temperature 450°C yielded surface carbonate species due to oxidation of the target molecules. The redox reaction was more prominent with the modified ZnO/In$_2$O$_3$ materials, thus accounting for the higher CO sensitivity.

DATA AVAILABILITY

All datasets generated for this study are included in the manuscript and/or the supplementary files.

AUTHOR CONTRIBUTIONS

AM, MR, and AG contributed to experimental work by materials synthesis, surface sites investigation, sensing tests, infrared measurements, and dissemination of the experimental data. MB and JH performed electron microscopy studies of materials and contributed to the manuscript preparation. NS, RS, BP, and DL contributed to the justification of the objectives of the study, discussion of experimental results and manuscript preparation.

FUNDING

SUPPLEMENTARY MATERIAL

The Supplementary Material for this article can be found online at: https://www.frontiersin.org/articles/10.3389/fmats.2019.00043/full#supplementary-material

REFERENCES

Atherton, K., Newbold, G., and Hockey, J. A. (1971). Infra-red spectroscopic studies of zinc oxide surfaces. *Discuss. Faraday Soc.* 52, 33–43. doi: 10.1039/df9715200033

Belokopytov, Y. U. V., Kholyavenko, K. M., and Gerei, S. V. (1979). An infrared study of the surface properties of metal oxides 2. the interaction of ammonia with the surface of Fe$_2$O$_3$, ZnO, MoO$_3$, and V$_2$O$_5$. *J. Catal.* 60, 1–7. doi: 10.1016/0021-9517(79)90061-7

Boccuzzi, F., Borello, E., Chiorino, A., and Zecchina, A. (1979). IR detection of surface microscopic modes of microcrystalline ZnO. *Chem. Phys. Lett.* 61, 617–619. doi: 10.1016/0009-2614(79)87186-9

Boccuzzi, F., Morterra, C., Scala, R., and Zecchina, A. (1981). Infrared spectrum of microcrystalline Zinc Oxide. electronic and vibrational contributions under different temperature and environmental conditions. *J. Chem. Soc. Faraday Trans.* 2, 2059–2066. doi: 10.1039/f29817702059

Chon, H., and Pajares, J. (1969). Hall effect studies of oxygen chemisorption on zinc oxide. *J. Catal.* 14, 257–260. doi: 10.1016/0021-9517(69)90433-3

Choo, T. F., Saidin, N. U., and Kok, K. Y. (2018). A novel self-heating zinc oxide/indium tin oxide based hydrogen gas sensor: dual sensing mode of hydrogen gas detection. *Chem. Phys. Lett.* 713, 180–184. doi: 10.1016/j.cplett.2018.10.043

Davydov, A. (2003). *Molecular Spectroscopy of Oxide Catalyst Surfaces.* Chichester: Wiley. doi: 10.1002/0470867981

Derakhshandeh, M., and Anaraki-Ardakani, H. (2016). A computational study on the experimentally observed sensitivity of Ga-doped ZnO nanocluster toward CO gas. *Physica E.* 84, 298–302. doi: 10.1016/j.physe.2016.06.026

Ellmer, K. (2010). "Transparent conductive zinc oxide and its derivatives," in *Handbook of Transparent Conductors*, ed D. S. Ginley (New York, NY: Springer), 193–265.

Espid, E., and Taghipour, F. (2017). Development of highly sensitive ZnO/In$_2$O$_3$ composite gas sensor activated by UV-LED. *Sens. Actuators B.* 241, 828–839. doi: 10.1016/j.snb.2016.10.129

Guo, L., Chen, F., Xie, N., Kou, X., Wang, C., Sun, Y., et al. (2018). Ultra-sensitive sensing platform based on Pt-ZnO-In$_2$O$_3$ nanofibers for detection of acetone. *Sens. Actuators B* 272, 185–194. doi: 10.1016/j.snb.2018.05.161

Han, N., Tian, Y., Wu, X., and Chen, Y. (2009). Improving humidity selectivity in formaldehyde gas sensing by a two-sensor array made of Ga-doped ZnO. *Sens. Actuators B* 138, 228–235. doi: 10.1016/j.snb.2009.01.054

Hjiri, M., Dhahri, R., El Mira, L., Bonavita, A., and Donato, N., Leonardi, S. G., et al. (2015). CO sensing properties of Ga-doped ZnO prepared by sol–gel route. *J. Alloys Comps.* 634, 187–192. doi: 10.1016/j.jallcom.2015.02.083

Hou, Y., and Jayatissa, A. H. (2014). Low resistive gallium doped nanocrystalline zinc oxide for gas sensor application via sol–gel process. *Sens. Actuators B* 204, 310–318. doi: 10.1016/j.snb.2014.07.082

Ilin, A. S., Ikim, M. I., Forsh, P. A., Belysheva, T. V., Martyshov, M. N., Kashkarov, P. K., et al. (2017). Green light activated hydrogen sensing of nanocrystalline composite ZnO-In$_2$O$_3$ films at room temperature. *Sci. Rep.* 7:12204. doi: 10.1038/s41598-017-12547-5

Keyes, B. M., Gedvilas, L. M., Li, X., and Coutts, T. J. (2005). Infrared spectroscopy of polycrystalline ZnO and ZnO:N thin films. *J. Cryst. Growth* 281, 297–302. doi: 10.1016/j.jcrysgro.2005.04.053

Kim, K., Song, Y.-W., Chang, S., Kim, I.-H., Kim, S., and Lee, S. Y. (2009). Fabrication and characterization of Ga-doped ZnO nanowire gas sensor for the detection of CO. *Thin Solid Films* 518, 1190–1193. doi: 10.1016/j.tsf.2009.03.229

Kołodziejczak-Radzimska, A., and Jesionowski, T. (2014). Zinc Oxide– from synthesis to application: a review. *Materials* 7, 2833–2881. doi: 10.3390/ma7042833

Korotcenkov, G., Brinzari, V., and Cho, B. K. (2016). In$_2$O$_3$- and SnO$_2$-Based Thin Film Ozone sensors: fundamentals. *J. Sens.* 2016:3816094. doi: 10.1155/2016/3816094

Lee, C.-S., Kim, I.-D., and Lee, J.-H. (2013). Selective and sensitive detection of trimethylamine using ZnO–In$_2$O$_3$ composite nanofibers. *Sens. Actuators B.* 181, 463–470. doi: 10.1016/j.snb.2013.02.008

Lee, S., Sun, G.-J., Lee, J. K., Hyun, S. K., and Lee, C. (2017). Enhanced ethanol gas sensing performance of the networked pd, In$_2$O$_3$-Codecorated ZnO Nanorod Sensor. *J. Korean Phys. Soc.* 71, 494–499. doi: 10.3938/jkps.71.494

Liang, Q., Xu, H., Zhao, J., and Gao, S. (2012). Micro humidity sensors based on ZnO–In$_2$O$_3$ thin films with high performances. *Sens. Actuators B.* 165, 76–81. doi: 10.1016/j.snb.2012.02.019

Lim, S. K., Hong, S. H., Hwang, S.-H., Choi, W. M., Kim, S., Park, H., et al. (2015). Synthesis of Al-doped ZnO nanorods via microemulsion method and their application as a CO gas sensor. *J. Mater. Sci. Technol.* 31, 639–644. doi: 10.1016/j.jmst.2014.12.004

Liu, F., Huang, G., Wang, X., Xie, X., Xu, G., Lu, G., et al. (2018). High response and selectivity of single crystalline ZnO nanorods modified by In$_2$O$_3$ nanoparticles for n-butanol gas sensing. *Sens. Actuators B.* 277, 144–151. doi: 10.1016/j.snb.2018.08.144

Ma, L., Fana, H., Tian, H., Fang, J., and Qian, X. (2016). The n-ZnO/n-In$_2$O$_3$ heterojunction formed by a surface-modification and their potential barrier-control in methanal gas sensing. *Sens. Actuators B.* 222, 508–516. doi: 10.1016/j.snb.2015.08.085

Marikutsa, A., Rumyantseva, M., Frolov, D., Morozov, I., Boltalin, A., Fedorova, A., et al. (2013). Role of PdO$_x$ and RuO$_y$ clusters in oxygen exchange between nanocrystalline tin dioxide and the gas phase. *J. Phys. Chem. C* 117, 23858–23867. doi: 10.1021/jp408646k

Markova, N., Berezina, O., Avdeev, N., and Pergament, A. (2018). UV sensitivity of indium-Zinc Oxide nanofibers. *Adv. Mater. Sci. Eng.* 2018:6351620. doi: 10.1155/2018/6351620

Morimoto, T., Yanal, H., and Nagao, M. (1976). Infrared spectra of ammonia adsorbed on Zinc Oxide. *J. Phys. Chem.* 80, 471–475. doi: 10.1021/j100546a010

Nakamoto, K. (1986). *Infrared and Raman Spectra of Inorganic and Coordination Compounds: Part A: Theory and Applications in Inorganic Chemistry*, 6th Edn. Hoboken, New Jersey: Wiley.

Nulhakim, L., Makinoa, H., Kishimoto, S., Nomoto, J., and Yamamoto, T. (2017). Enhancement of the hydrogen gas sensitivity by large distribution of c-axis preferred orientation in highly Ga-doped ZnO polycrystalline thin films. *Mater. Sci. Semicondu. Process.* 68, 322–326. doi: 10.1016/j.mssp.2017.06.045

Pearton, S. J., Norton, D. P., Ip, K., Heo, Y. W., and Steiner, T. (2005). Recent progress in processing and properties of ZnO. *Progress Mater. Sci.* 50, 293–340. doi: 10.1016/j.pmatsci.2004.04.001

Phan, D.-T., and Chung, G.-S. (2013). Effects of defects in Ga-doped ZnO nanorods formed by a hydrothermal method on CO sensing properties. *Sens. Actuators B.* 187, 191–197. doi: 10.1016/j.snb.2012.10.080

Rambu, A. P., Sirbu, D., Iftimie, N., and Rusu, G. I. (2011). Polycrystalline ZnO–In$_2$O$_3$ thin films as gas sensors. *Thin Solid Films* 520, 1303–1307. doi: 10.1016/j.tsf.2011.04.158

Saniz, R., Sarmadian, N., Partoens, B., Batuk, M., Hadermann, J., Marikutsa, A., et al. (2018). First-principles study of CO and OH adsorption on In-doped ZnO surfaces. *arXiv:1806.01338.*

Saussey, J., Lavalley, J.-C., and Bovet, C. (1982). Infrared study of CO$_2$ adsorption on ZnO. Adsorption sites. *J. Chem. Soc. Faraday Trans.* 1, 1457–1463. doi: 10.1039/f19827801457

Shannon, R. D. (1976). Revised effective ionic radii and systematic studies of interatomic distances in halides and chalcogenides. *Acta Cryst. A* 32, 751–767. doi: 10.1107/S0567739476001551

Singh, N., Ponzoni, A., Gupta, R. K., Lee, P. S., and Comini, E. (2011). Synthesis of In$_2$O$_3$-ZnO core–shell nanowires and their application in gas sensing. *Sens. Actuators B* 160, 1346–1351. doi: 10.1016/j.snb.2011.09.073

Trakhtenberga, L. I., Gerasimov, G. N., Gromov, V. F., Belysheva, T. V., and Ilegbusi, O. J. (2013). Conductivity and sensing properties of In$_2$O$_3$ + ZnO mixed nanostructured films: Effect of composition and temperature. *Sens. Actuators B.* 187, 514–521. doi: 10.1016/j.snb.2013.03.017

Vorobyeva, N., Rumyantseva, M., Filatova, D., Konstantinova, E., Grishina, D., Abakumov, A., et al. (2013). Nanocrystalline ZnO(Ga): Paramagnetic centers, surface acidity and gas sensor properties. *Sens. Actuators B* 182, 555–564. doi: 10.1016/j.snb.2013.03.068

Vorobyeva, N., Rumyantseva, M., Filatova, D., Spiridonov, F., Zaytsev, V., Zaytseva, A., et al. (2017). Highly Sensitive ZnO(Ga, In) for Sub-ppm level NO$_2$ detection: effect of indium content. *Chemosensors* 5:18. doi: 10.3390/chemosensors5020018

Wang, B., Jin, H. T., Zheng, Z. Q., Zhou, Y. H., and Gao, C. (2017). Low-temperature and highly sensitive C$_2$H$_2$ sensor based on Au decorated ZnO/In$_2$O$_3$ belt-tooth shape nano-heterostructures. *Sens. Actuators B* 244, 344–356. doi: 10.1016/j.snb.2016.12.044

Wang, Z., Huang, B., Dai, Y., Qin, X., Zhang, X., Wang, P., et al. (2009). Highly photocatalytic ZnO/In2O3 heteronanostructures synthesized by a coprecipitation method. *J. Phys. Chem. C* 113, 4612–4617. doi: 10.1021/jp8107683

Wei, N., Cui, H., Wang, X., Xie, X., Wang, M., Zhang, L., et al. (2017). Hierarchical assembly of In$_2$O$_3$ nanoparticles on ZnO hollow nanotubes using carbon fibers as templates: Enhanced photocatalytic and gas sensing properties. *J. Colloid Interface Sci.* 498, 263–270. doi: 10.1016/j.jcis.2017.03.072

Zou, X., Yan, X., Li, G., Tian, Y., Zhang, M., and Liang, L. (2017). Solution combustion synthesis and enhanced gas sensing properties of porous In$_2$O$_3$/ZnO heterostructures. *RSC Adv.* 7:34482. doi: 10.1039/C7RA04852A